

Analysis of the directionality on periodic materials

Nicolás Guarín-Zapata^a, Camilo Valencia^a, Juan Gomez^b

^aUniversidad EAFIT, School of Applied Sciences and Engineering, Medellín 050022, Colombia

^bRisk and Design Consulting, Medellín 050022, Colombia

ARTICLE HISTORY

Compiled July 6, 2023

ABSTRACT

There is an increasing interest in the study of metamaterials and periodic materials across disciplines. These are anisotropic and their properties present directionality. For example, the wave speed depends on the propagation direction. Furthermore, they are heterogeneous, and their directionality depends on their spectra. Common approaches to describe anisotropy have been used in the large-wavelength approximation corresponding to static properties. Here we present an anisotropy measure based on the dynamic behavior. It receives dispersion surfaces from Bloch analyses and outputs a curve/surface with bulk directionality encoded on it. We present results for elastodynamics, but it is applicable to other phenomena.

KEYWORDS

Periodic material; phononic crystal; dispersion relation; Bloch analysis; anisotropy

1. Introduction

Across disciplines, there is a growing interest in the research and design of metamaterials and periodic materials [1–3]. The emergence of unusual properties such as effective negative mass, negative refraction, negative Poisson ratio, and acoustic/electromagnetic cloaking has piqued the attention of scientists [4–6]. As a result, there is a trend in designing microstructures to control bulk properties [7–11]. Although direct numerical simulations of the bulk of the material and the entire microstructure are feasible [12], the most common method is to take advantage of the material's periodicity and model a single cell [5,13]. This is accomplished using Bloch's theorem [14]. Bloch's theorem was developed in solid-state physics [15,16], but it has since been applied to electrodynamics [2], acoustics [3,17], and elastodynamics [5,18,19].

Periodic materials are anisotropic because of discrete symmetries in their unit cells [16,20–22]. This anisotropy behavior translates into directionality in wave propagation, i.e., the speed of waves depends on the direction of propagation. If we want to study the propagation of waves in a periodic material, we are interested in characterizing this directionality. Furthermore, due to the heterogeneous nature of periodic materials,

This is an original manuscript of an article published by Taylor & Francis in *Mechanics of Advanced Materials and Structures* on 02 Jul 2023, available at: <https://doi.org/10.1080/15376494.2023.2226958>

Juan Gómez was formerly at Universidad EAFIT

CONTACT: Nicolás Guarín-Zapata. Email: nguarinz@eafit.edu.co

their anisotropy depends on the frequency of the waves propagating through them. That is, we could talk of a *dynamically induced anisotropy*. This behavior has been reported in the literature [23,24] and is related with the interaction of the waves and the microstructure. Mediated by the relation between the wavelengths and characteristic length in the material. We illustrate this phenomenon with a 2D mass-spring lattice, where we can compute the solution analytically.

There have been some efforts in defining descriptors that quantify the anisotropy level of materials [25–27], they are not perfect because they reduce all the information to a single number and do not provide information about the preferred direction of propagation or symmetries present. Guarán-Zapata et al. [11] used a qualitative approach to compare anisotropy for different transversely isotropic materials and select them to tune the behavior of helicoidal composites. This was used for transversely isotropic materials, where the dispersion relations can be obtained analytically [28] and used to analyze a single layer of a composite. For heterogeneous materials and materials with other symmetries besides isotropy and transverse isotropy, this type of information is not available analytically and numerical simulations are required. Thus, a general tool to analyze the bulk anisotropy of materials is desired.

Here we present a new anisotropy measure based on the dynamic behavior of the material. Our approach takes as input dispersion (hyper-) surfaces obtained using a Bloch analysis and outputs a curve/surface with the bulk directionality encoded on it. We present some results for the case of elastodynamics, but they are directly applicable to problems with other underlying physical phenomena. As such, this method allows extending directionality analyses in metamaterials and periodic materials beyond the long wavelength regime.

This paper introduces a novel anisotropy measure based on the dynamic behavior of the material. As such, it considers the material’s heterogeneity and works beyond the long-wavelength regime. The method can be applied to a specific frequency or any chosen frequency range. The starting point is dispersion (hyper-) surfaces, which are a common result when applying Bloch’s theorem to periodic materials. We begin with some generalities about periodic materials and Bloch’s theorem, which is used to describe bulk behavior with a single unit cell. Then, we describe the propagation of waves in anisotropic elastic materials in two and three dimensions. Following this section, we present the suggested method for analyzing periodic material directionality, as well as some tests for the method in analytically and numerically obtained dispersion relations. Although all the examples presented are from the area of elastodynamics, this method applies to any material that employs dispersion (hyper-) surfaces as input, such as electrodynamics or quantum mechanics.

2. Periodic materials

A periodic material is defined by the spatial repetition of a given motif in one, two, or three dimensions. The motifs refer to heterogeneities in the material properties at the microstructural level and can contain different materials, topologies, and shapes. For example, in the case of electromagnetic waves, we have *photonic crystals* and the periodicity of electric permittivity and magnetic permeability [2]. For elastic waves, the term is *phononic crystals* and we have periodicity in the stiffness and mass density of the material [3]. Such periodic materials are described by a lattice and by an elementary unit cell. Figures 1(a)–1(c) show a three-dimensional material with periodicity in one, two, and three dimensions. A set of base vectors defines the lattice (Fig. 1(d)).

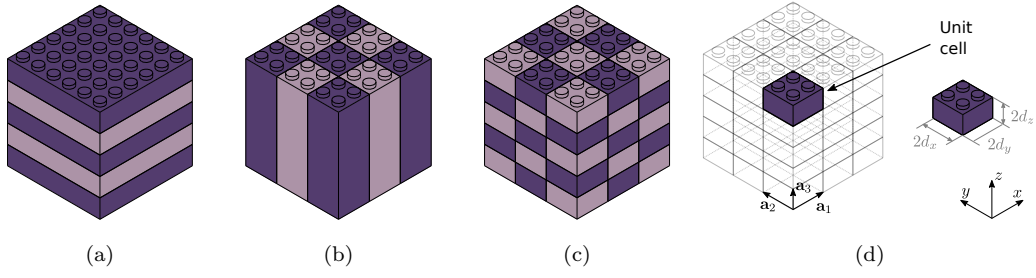


Figure 1. 3D material with different periodicities. Regardless of the space dimensionality its periodicity could be in (a) one (b) two or (c) three space dimensions. (d) The purple lego-brick defines the fundamental unit cell which allows construction or filling of space after applying translation operations according to the lattice vector \mathbf{a} .

These allow the construction of the whole material through successive applications of translation operations of the unit cell. To study this type of material it is common to take advantage of the periodicity of the material properties and express the solution using Bloch's theorem [15].

2.1. Bloch's theorem

Let us consider a generalized wave equation of the form

$$\mathcal{L}\mathbf{u}(\mathbf{x}) = -\omega^2\mathbf{u}(\mathbf{x}), \quad (1)$$

where \mathcal{L} is a positive definite operator [29,30], \mathbf{u} is the field of interest, and ω is the angular frequency. Bloch's theorem establishes that solutions to (1) are of the form

$$\mathbf{u}(\mathbf{x}) = \mathbf{w}(\mathbf{x})e^{i\boldsymbol{\kappa}\cdot\mathbf{x}}, \quad (2)$$

where $\mathbf{w}(\mathbf{x})$ is a function with the same periodicity of the material. Opposite sides of the unit cell are separated by a vector \mathbf{a} and, as a consequence,

$$\mathbf{u}(\mathbf{x} + \mathbf{a}) = \mathbf{u}(\mathbf{x})e^{i\boldsymbol{\kappa}\cdot\mathbf{a}}.$$

The expressions $\mathbf{u}(\mathbf{x} + \mathbf{a})$ and $\mathbf{u}(\mathbf{x})$ give the field at $\mathbf{x} + \mathbf{a}$ and \mathbf{x} , while $\mathbf{a} = \mathbf{a}_1n_1 + \mathbf{a}_2n_2 + \mathbf{a}_3n_3$ is the lattice translation vector shown in Figure 1(d). The term $e^{i\boldsymbol{\kappa}\cdot\mathbf{a}}$ represents a phase shift between opposite sides of the unit cell. This relationship between opposite sides of the fundamental cell stated in the theorem through the boundary terms permits the characterization of the fundamental properties of the material with the analysis of a single cell.

Computationally, equation (1) is commonly translated to a generalized eigenvalue problem through a numerical method such as the Finite Element Method. And we end up with a system of the form

$$[K]\{\mathbf{U}\} = \omega^2[M]\{\mathbf{U}\},$$

where $[K]$ is the stiffness matrix and $[M]$ is the mass matrix. Bloch's theorem can be applied through boundary conditions imposed strongly by directly including the phase

shifts at the element level or performing row and column operations in these matrices [18]; or weakly imposing them through Lagrange multipliers or penalty methods [31, 32]. After this process, we end up with the following system

$$[K_R(\boldsymbol{\kappa})]\{\mathbf{U}_R\} = \omega^2[M_R(\boldsymbol{\kappa})]\{\mathbf{U}_R\},$$

where \mathbf{k} is the wave vector which, is progressively assigned successive values, in such a way that the first Brillouin zone is fully covered. Each evaluation for a particular wave vector and the solution of the related eigenvalue problem yields tuples of the form (\mathbf{k}, ω_n) representing a plane wave propagating at frequency ω_n . The subindex n refers to the n th eigenvalue computed for the input wave vector $\boldsymbol{\kappa}$; this is depicted in Figure 2.

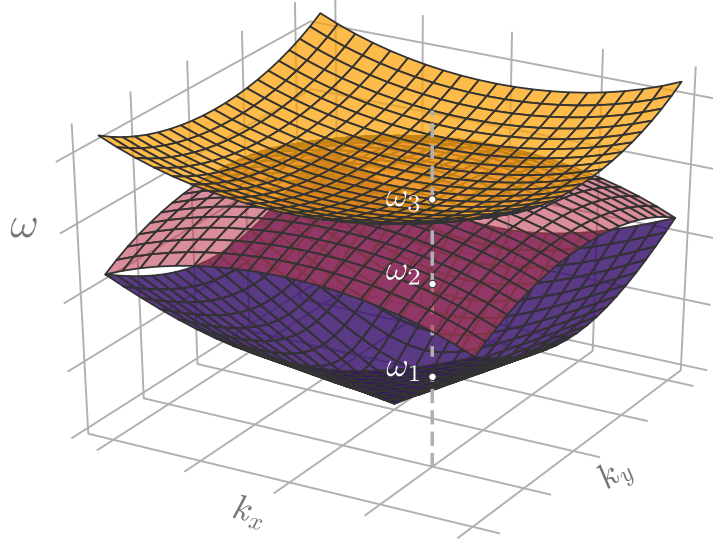


Figure 2. Schematic depicting the multiple branches obtained in a Bloch analysis. For a single point in the wavevector space there are multiple values for the frequency.

Having multiple dispersion surfaces is common for problems in electrodynamics or elastodynamics [1,2]. This is a consequence of the vector nature of the physical quantities of interest: electric/magnetic field or displacement vector, respectively. In the case of homogeneous materials, we have two transverse modes for electromagnetic waves and two transverse modes plus a longitudinal one for elastic waves. Nevertheless, Bloch analysis introduces an additional complication since the computations are done in the first Brillouin zone. Here, wavevectors are determined up to an additive constant that is written in terms of the lattice vectors

$$\mathbf{a}_1 n_1 + \mathbf{a}_2 n_2 + \mathbf{a}_3 n_3 \quad \forall n_1, n_2, n_3 \in \mathbb{Z}.$$

This means that we map the vectors $\boldsymbol{\kappa}$ and $\boldsymbol{\kappa} + \mathbf{a}_1 n_1 + \mathbf{a}_2 n_2 + \mathbf{a}_3 n_3$ to the same point in the first Brillouin zone. Figure 3 illustrates this effect for the first three dispersion surfaces in the case of a homogeneous material.

As shown in Figure 3, when using Bloch analysis, we obtain dispersion surfaces ordered by frequency. This might lead to conclude that materials are anisotropic when

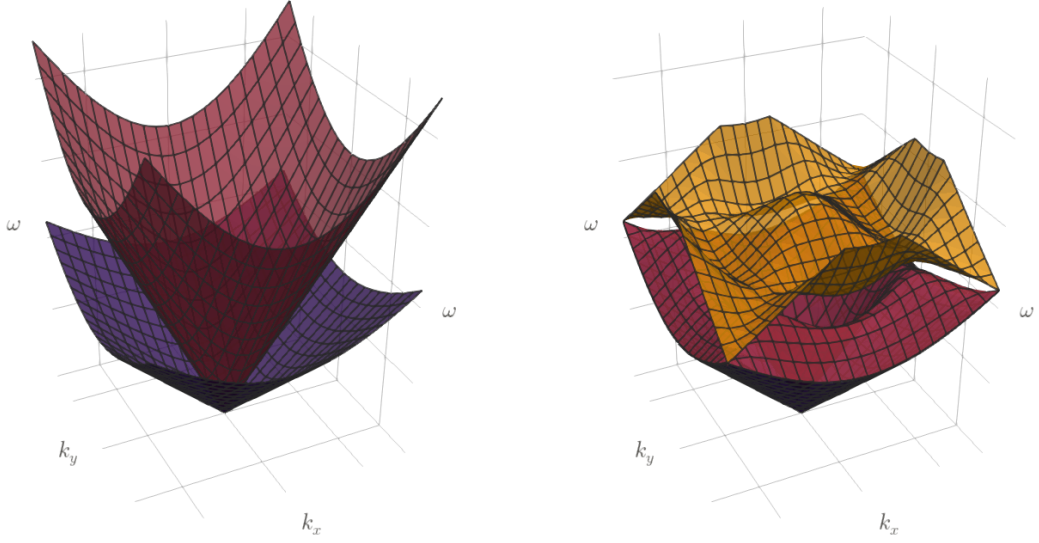


Figure 3. Comparison of the dispersion surfaces for a homogeneous material computed with the classical expression (left) with the dispersion surfaces obtained using Bloch analysis (right). Here we are showing the first three branches.

they are not, as illustrated in Figure 4. For low wavenumbers, we can see that the material is isotropic/anisotropic when looking at the first mode. Nevertheless, this is not the case when looking at the second and third modes. Furthermore, anisotropy in one material might be more pronounced in one propagation mode than in others.

This apparent anisotropy is more difficult to analyze if we consider wave propagation in three dimensions instead of two, as can be seen in Figure 5.

3. Elastic wave propagation in anisotropic media

As mentioned before, periodic materials are inherently anisotropic due to their microstructure. Their *level* of anisotropy obeys the symmetries present. In this section we describe the propagation of waves for elastic solids of general anisotropy.

Let us consider a wave that propagates in a solid. In this case, the conservation of density of momentum in the absence of body forces is written as

$$\sigma_{ij,i} = \rho \frac{\partial^2 u_i}{\partial t^2},$$

with σ_{ij} the stress tensor, u_i the displacement vector, and ρ the mass density. In the case of a linear elastic material, Hooke's law is given by

$$\sigma_{ij} = c_{ijkl} u_{k,l},$$

where c_{ijkl} is the stiffness tensor that can have up to 21 constants in the case of general anisotropy.

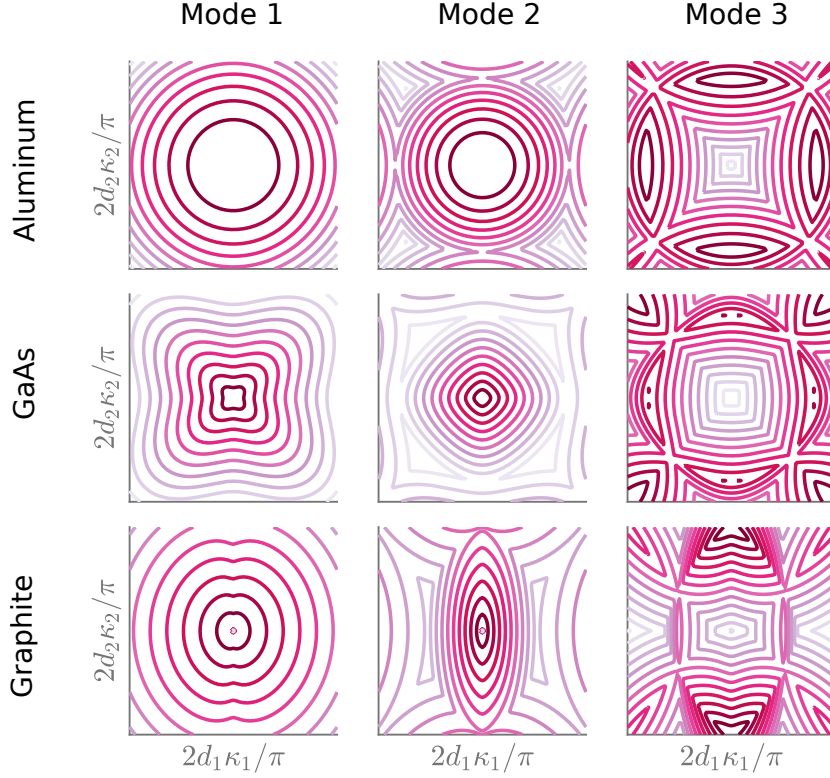


Figure 4. Comparison of the contours of iso-frequency for the first three dispersion modes for isotropic, cubic and orthotropic materials. **(Top)** Contours for aluminum, an isotropic example. **(Middle)** Contours for GaAs, a cubic example. **(Bottom)** Contours for graphite, an orthotropic example.

If we assume a plane-wave solution of the form

$$u_j = U_j e^{i\kappa(n_m x_m - v_p t)};$$

where $\kappa = |\boldsymbol{\kappa}|$ is the wavenumber, n_m is a unit vector in the direction of $\boldsymbol{\kappa}$, and v_p is the phase speed; we end up with the Christoffel wave equation [28,33,34]:

$$[\Gamma_{ij} - \rho v_p^2 \delta_{ij}] U_j = 0,$$

where $\Gamma_{ij} = c_{ijkl} n_k n_l$ is the Christoffel stiffness tensor or acoustic tensor, and δ_{ij} is the Kronecker delta. This is an eigenvalue problem with eigenvalues ρv_p^2 . Here, v_p represents the phase speeds of the material. The corresponding characteristic polynomial is

$$\det[\Gamma_{ij} - \rho v_p^2 \delta_{ij}] = 0. \quad (3)$$

From (3) we conclude that there are three propagating waves, each one with a different polarization. These directions are orthogonal since Γ_{ij} is symmetric. Of the three polarizations, we have two quasi-transverse (qS) waves and one quasi-longitudinal (qP) wave. Where the prefix *quasi* implies that two of the modes are close to orthogonal to the wavevector and the other is close to parallel to it. As we can see, the value of Γ_{ij}

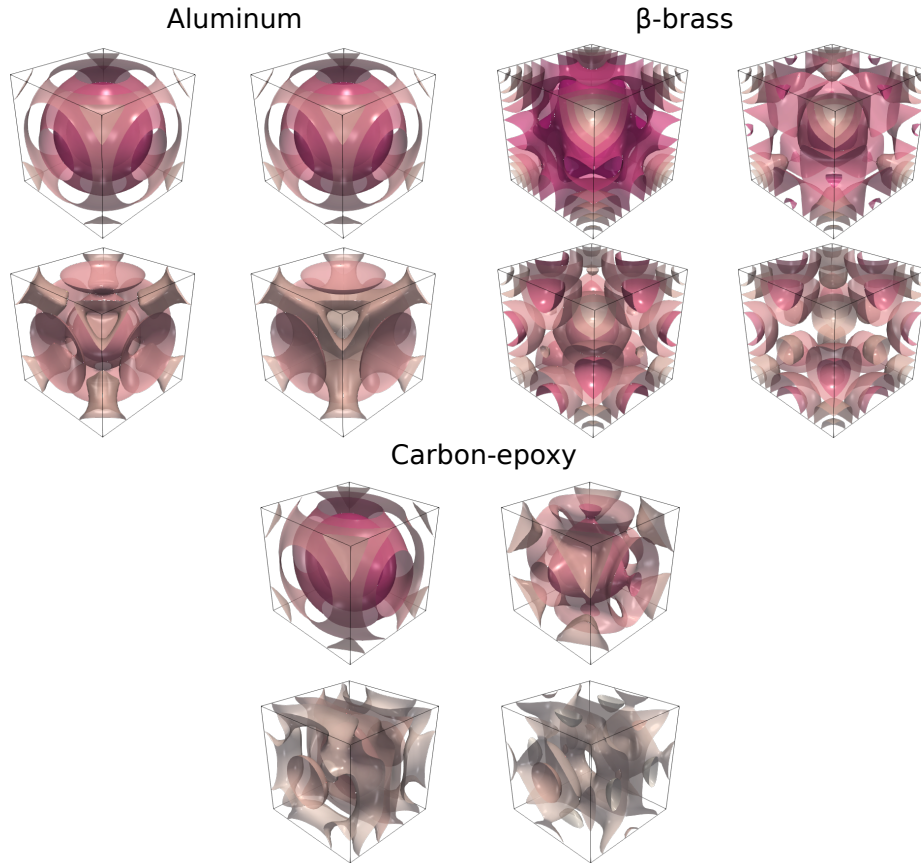


Figure 5. Comparison of the the first four dispersion modes for isotropic, cubic, and transverse isotropic materials. The surfaces represent iso-frequency values for the dispersion relations.

depends on the direction of propagation implying that the phase speed depends on the direction of the wave. This effect is represented in Figure 6, where we are visualizing the phase speed for two anisotropic materials: β -brass and carbon-epoxy.

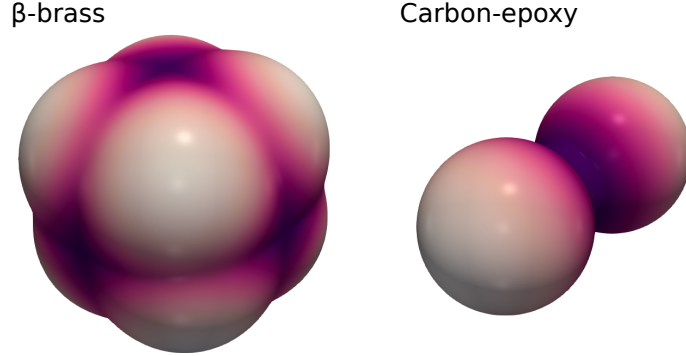


Figure 6. Comparison of the directionality of the phase speed for quasi-longitudinal (qP) modes for a cubic (left) and transverse isotropic material (right).

We can rewrite (3) as

$$\Omega(\omega, \boldsymbol{\kappa}) = \det \left[\Gamma_{ij} - \rho \frac{\omega^2}{\|\boldsymbol{\kappa}\|^2} \delta_{ij} \right], \quad (4)$$

considering that the phase speed is defined as $v_p^2 = \omega^2 / \|\boldsymbol{\kappa}\|^2$. The group velocity is defined as [28]

$$\mathbf{v}_g = \frac{\nabla_{\boldsymbol{\kappa}} \Omega}{\partial \Omega / \partial \omega}, \quad (5)$$

and for lossless media it represents the direction of energy flow.

4. Evaluation of directionality

Elastic anisotropy plays a role in different applications such as metallurgy [25], geophysics [35], wave propagation in composites [11], and metamaterials [36], among others. Thus, for a particular application, one might need a material with more or less anisotropy, and the question of how anisotropic different materials are arises naturally.

4.1. Dynamically induced anisotropy

As mentioned before, in periodic material their anisotropy depends on the frequency of the waves propagating through them [23,24]. That is, there exists a dynamically induced anisotropy that relates to the interaction of the waves and the microstructure. We can contrast this case with the static case. Which corresponds to the large-wavelength approximation of the dynamic case.

To illustrate this phenomenon, here we present as an example the dispersion for a 2D mass-spring lattice. Figure 7 presents the unit cell for this lattice.

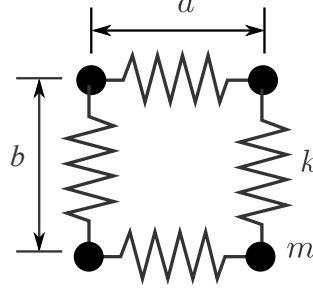


Figure 7. Unit cell for a 2D mass spring lattice. Here k is the stiffness of the spring, m is the mass, a is the distance between neighbors in the x -direction, and b is the distance between neighbors in the y direction.

The analytic solution, in this case, is the following — see [5] for a deduction of this solution:

$$\Omega^2 = 2[2 - \cos(\kappa_1 a/\pi) - \cos(\kappa_2 b/\pi)],$$

where $\Omega = \omega/\omega_0$ is the normalized frequency, $\omega_0 = \sqrt{k/m}$ is the frequency for a single spring-mass system, κ_1 is the wave number in the x -direction, κ_2 is the wave number in the y -direction, a is the distance between neighbors in the x -direction, and b is the distance between neighbors in the y direction. Figure 8 presents the dispersion relation for this problem.

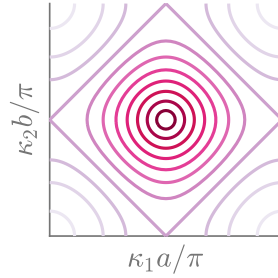


Figure 8. Iso-frequency contours for the dispersion relation in the spring-mass lattice.

If we analyze the directionality for this problem, we see that for low frequency it seems to be isotropic, but it starts to turn anisotropic when the frequency is changed. This is depicted in Figure 9. We have different normalized frequencies: $\Omega = 0.5$, $\Omega = 1.0$, $\Omega = 1.5$, and $\Omega = 1.99$. For this particular problem, the maximum propagating frequency is $\Omega = 2$.

4.2. Some existing measures of anisotropy

One of the first measures of anisotropy was the Zener ratio [25] which is defined for cubic materials and is written as

$$a_r = \frac{2C_{44}}{C_{11} - C_{12}}.$$

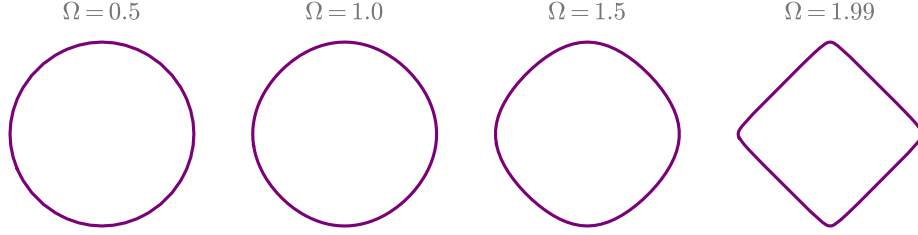


Figure 9. Comparison of the directionality for a spring-mass lattice for different normalized frequencies $\Omega = 0.5$, $\Omega = 1.0$, $\Omega = 1.5$, and $\Omega = 1.99$.

From an intuitive perspective, it is defined as the ratio between the classical shear modulus and the *new one* that appears in cubic materials. The Zener ratio is one for isotropic materials. One extension of the Zener ratio for materials with more general anisotropy replaces the elastic coefficients by averages while retaining the form of the original ratio [26]

$$a_{\text{gen}} = \frac{2Y_{44}}{Y_{11} - Y_{12}},$$

with

$$Y_{11} = \frac{C_{11} + C_{22} + C_{33}}{3}, Y_{12} = \frac{C_{12} + C_{23} + C_{13}}{3}, Y_{44} = \frac{C_{44} + C_{55} + C_{66}}{3}.$$

There are other proposed metrics for measuring anisotropy such as the ratio of the maximum and minimum phase speed for the quasi-transverse modes [37] or the norm of the projection to the closest isotropic tensor [34]. Ranganathan and Ostoja-Starzewski [27] compute some of these metrics for several crystals and compare them with a new metric termed universal anisotropy index (UAI). Although these metrics seem to be usable for general anisotropic materials they were conceived with homogeneous materials in mind.

Regarding the anisotropy of composites, it is common to present the directionality as group velocity polar histograms based on iso-frequency contours [23,24]. Furthermore, Casadei and Rimoli [36] computed an anisotropy index considering each propagation mode separately. This measure is, essentially, the standard deviation for each wave propagation mode. The main drawback with these approaches is that they considered just the first two or three modes of propagation, that is, low frequencies. Since phononic crystals can present dispersion, it is expected that the anisotropy (directionality) depends on the frequency.

4.3. Method for directionality

Valencia et al. [10] proposed a method to characterize the directionality of phononic crystals that considers the contribution of multiple modes, not just the low-frequency ones as in previous works [23,24]. Thus, the approach allows a more complete description of the directional response in a material and is valid in the low and high-frequency

regimes. They defined the wave propagation directionality, D , as

$$D = \sum_{\substack{i \\ e > \text{tol}}} d_i(\theta), \quad d_i(\theta) = C(\nabla M_i) \quad (6)$$

where M_i is the i th mode in the dispersion relation, ∇M_i is its gradient with respect to the wavevector κ , tol is a predefined tolerance, $\theta = [0, 2\pi]$ is the angle defining the propagation direction. In this definition, the operator C associates each vector to its direction (θ) and adds it to the previous vector sharing the same direction. Consequently, $d_i = C(\nabla M_i)$ corresponds to a weighted polar histogram representing the distribution of group velocity for mode M_i in any propagation direction. The weight is given by the number of times a particular direction appears in the (discrete) dispersion relations. We can summarize this method as:

- Start from the frequency surface and compute the gradient to obtain group velocities.
- Sort the (discrete) gradient by angle and add their magnitudes when they share the angle.

These steps are depicted in Figure 10.

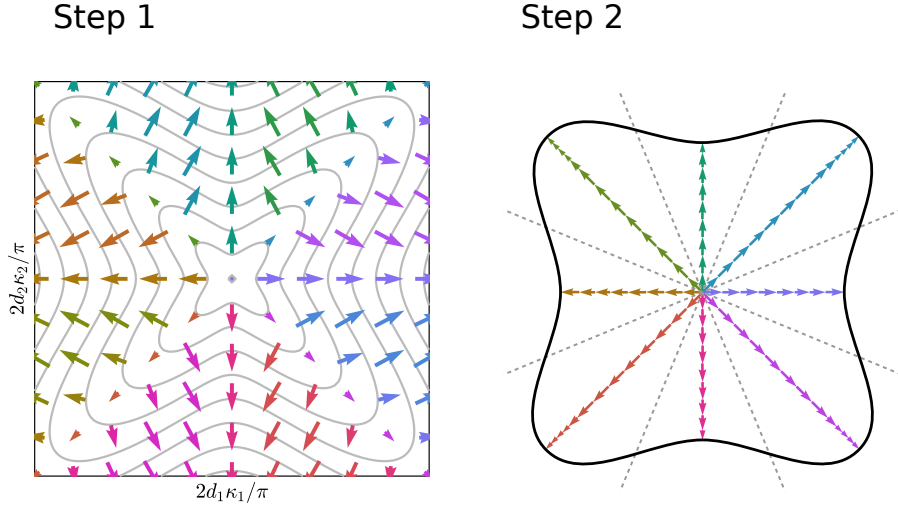


Figure 10. In **Step 1** we compute the gradient of the the i th mode of the dispersion curve. Then, in **Step 2** the group velocity vectors are rearranged according to their direction and added. The resulting envelope curve represents the directionality for that mode.

One problem with this method is that it considers group velocity vectors for regions with wavevectors of different magnitudes. For example, when considering a square unit cell it will include more vectors associated to directions $(1, 1)$, $(-1, 1)$, $(-1, -1)$ and $(1, -1)$. This makes the method dependent on the choice of the unit cell shape. Our proposed improvement is to average vectors instead of accumulating them. This is similar to restricting the analysis to wavevectors enclosed by a sphere with constant wavevector magnitude—in solid state physics states enclosed by a constant-energy surface are considered to compute the density of states [16]. As an example, let us compare the computed directionality for the first dispersion branch. That is, the first

eigenvalue obtained from the Bloch analysis of the unit cell. This is shown in Figure 11.

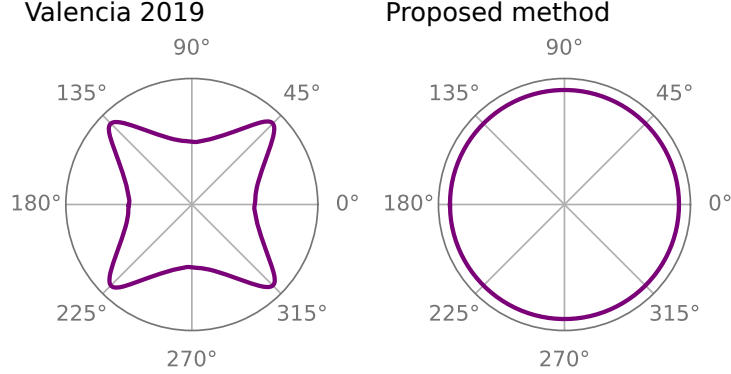


Figure 11. Comparison of the computed directionality for the first dispersion branch in a homogeneous material using (left) [10] method and (right) our approach.

Thus, we can summarize the modified method with the following steps:

- Start from the frequency surface and compute the gradient to obtain group velocities.
- Sort the (discrete) gradient by angle and average their magnitudes when they share the angle.

One natural question that follows is how to extend the method to three dimensions. But when going from two to three dimensions we do not have a uniform partition of the sphere. A polyhedron where the vertices of the faces are uniformly distributed over a spherical surface. In comparison with two dimensions. Where we used a uniform partition of the circle to sample the directions for group velocities. In the three-dimensional case, we could parameterize the sphere using spherical coordinates, for example. This would represent a problem for our method since there is a higher density of polygons in the poles. We expect this because the area differential in spherical coordinates is given by $dA = r \sin \theta d\varphi d\theta$ — here, θ is the zenithal angle and φ the azimuthal angle [38]. To avoid this problem, we used a triangulated mesh for the sphere that is close to uniform [39]. Figure 12 provides a comparison of two meshes: one using spherical coordinates and the other with a sampling that is close to uniform.

Another difference that poses a challenge to extend the method from two to three dimensions is the absence of a *natural* order for the points¹. To address this issue, we computed the spherical angles for each point in the sphere and created a k-D tree [40,41]. Then, at the moment of evaluating the direction of each group velocity vector, we made a nearest-neighbor search for its angles (θ, φ) to assign the vector to a point on the sphere as was done in the two-dimensional case.

¹The preimage of the circle (1D) is an ordered set, that is, an interval—that follows the order of the real numbers. We cannot define this relation directly for the preimage of a sphere (2D).

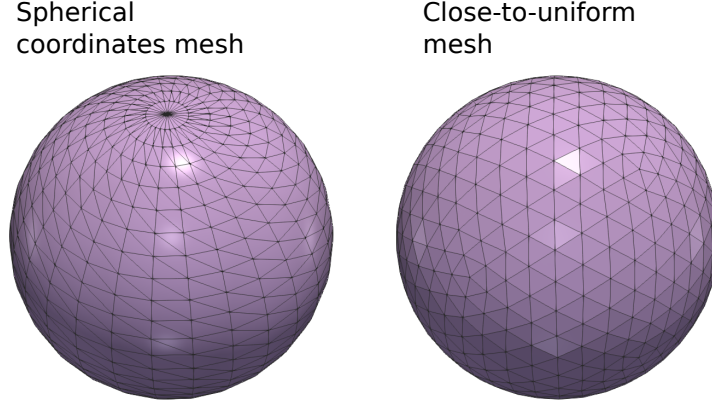


Figure 12. Comparison of a mesh of a sphere using a mesh that follows spherical coordinates and a close-to-uniform mesh. Notice the higher density of element in the pole of the left mesh.

5. Results

To test the method, we computed the directionality for materials with different symmetry classes in two and three dimensions. First, we test the method using homogeneous materials that allow us to (semi) analytically obtain the dispersion relations and then we try it with results obtained using the finite element method for a micropolar elastic material. That also shows that the method does not depend on the equations being analyzed and only needs the dispersion relations as input.

5.1. Results for analytic dispersion relations

We want to solve the determinant in (4) for ω to determine the dispersion relations. We rewrite the equation for completeness,

$$\Omega(\omega, \boldsymbol{\kappa}) = \det \left[\Gamma_{ij} - \rho \frac{\omega^2}{\|\boldsymbol{\kappa}\|^2} \delta_{ij} \right] = 0.$$

This corresponds to solving a third-degree polynomial equation for each wavenumber $\boldsymbol{\kappa}$ (see the appendix at the end of this chapter for explicit forms of these equations). Then, for homogeneous materials, these relations can be solved semi-analytically and can be written as

$$\omega \equiv \omega(\boldsymbol{\kappa}).$$

On the other hand, when these relationships are obtained from Bloch's theorem the dispersion relationships also contain information from different Brillouin zones leading to relations of the form

$$\omega_{m_1, m_1} \equiv \omega(\boldsymbol{\kappa}_{m_1, m_2}), \tag{7}$$

in two dimensions, where the subscripts m_1, m_2 correspond to integer numbers referring to waves coming from adjacent Brillouin zones. In the case of three dimensions

the relations are of the form

$$\omega_{m_1, m_2, m_3} \equiv \omega(\boldsymbol{\kappa}_{m_1, m_2, m_3}). \quad (8)$$

In the case of a square/cube unit cell with side d , we have the following generalized definition of the wavevector [42]:

$$\boldsymbol{\kappa}_{m_1, m_2} = \left(\kappa_x + \frac{m_1 \pi}{d}, \kappa_y + \frac{m_2 \pi}{d} \right), \quad (9)$$

$$\boldsymbol{\kappa}_{m_1, m_2, m_3} = \left(\kappa_x + \frac{m_1 \pi}{d}, \kappa_y + \frac{m_2 \pi}{d}, \kappa_z + \frac{m_3 \pi}{d} \right), \quad (10)$$

where κ_x , κ_y , and κ_z are the components of the wave vector.

Figure 13 presents a comparison of directionality for a periodic material with a square unit cell for aluminum (isotropic), GaAs (cubic) and Graphite (orthotropic). Here, we obtained the dispersion curves analytically and restrict them to the First Brillouin Zone using (9). We can see that the directionality curves present the same symmetries than the material class in each case (see the appendix at the end for the material properties). The curve corresponding to the isotropic material is (almost) symmetric with respect to any rotation in the plane. In the case of the cubic material, the curve remains the same after rotations of 90° . Finally, for the orthotropic material, we can see two planes of symmetry corresponding to the x and y axes.

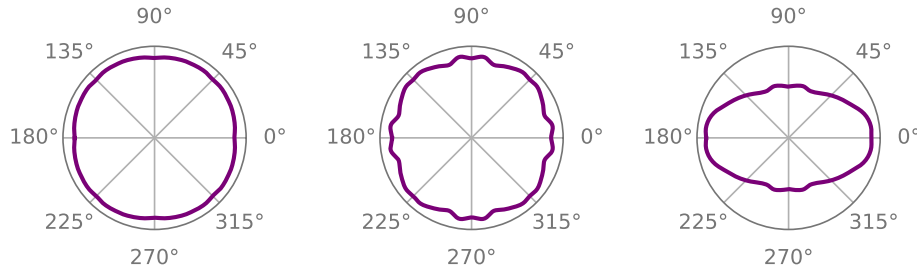


Figure 13. Comparison of directionality for a periodic material with a square unit cell for isotropic, cubic, and orthotropic materials. We obtained the dispersion curves analytically and restricted them to the First Brillouin Zone using (9) **(Left)** Directionality for aluminum, an isotropic example. **(Center)** Directionality for GaAs, a cubic example. **(Right)** Directionality for graphite, an orthotropic example.

Figure 14 presents a comparison of directionality for a periodic material made of β -brass (cubic) and cadmium (transverse isotropic). For the cubic material figure 14 presents a top view and an isometric view of the surface, the frontal and lateral views are omitted since it presents a symmetry with respect to rotations of 90° . In the case of the transverse isotropic material a third-angle projection plus the isometric view are presented. We can see that the directionality surfaces present the same symmetries as the material class in each case. In particular, the surface is (almost) symmetric with respect to the z -axis (see the appendix at the end for the material properties used).

5.2. Results for numerically-obtained dispersion relations

As a final result, we computed the directionality curves for cellular materials with circular pores. We changed the diameter of the pore while the size of the cell is kept

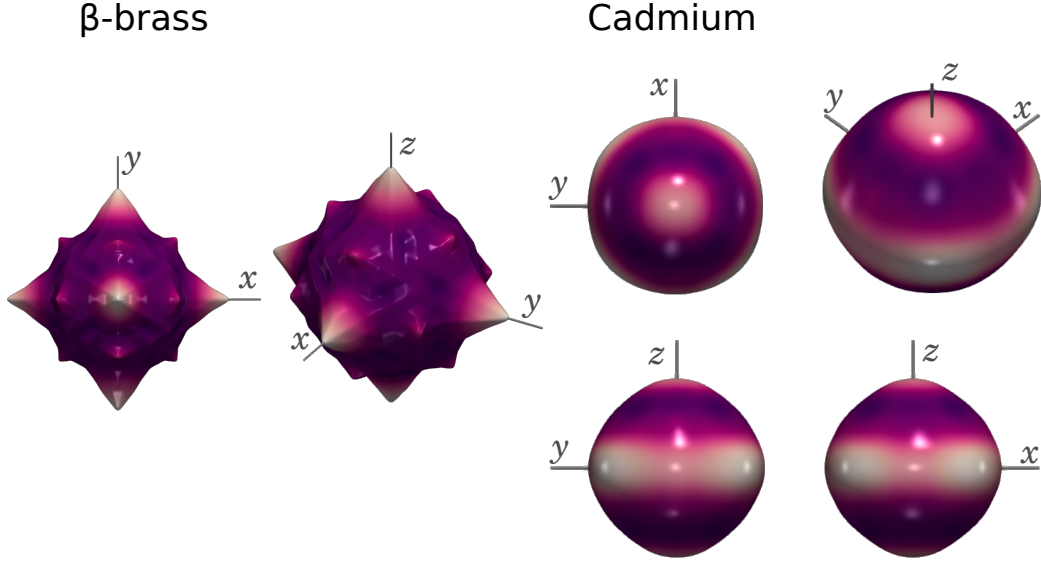


Figure 14. Comparison of the directionality surfaces for (**Left**) β -brass (**Right**) and cadmium.

fixed. The material used is a micropolar one with the following properties [19]:

$$\begin{aligned}
 \rho &= 2770 \text{ kg/m}^3, & \lambda &= 5.12 \times 10^{10} \text{ Pa}, \\
 \mu &= 2.76 \times 10^{10} \text{ Pa}, & \alpha &= 3.07 \times 10^9 \text{ Pa}, \\
 \gamma + \epsilon &= 7.66 \times 10^{10} \text{ N}, & J &= 306.5 \text{ kg/m}.
 \end{aligned}$$

where ρ is the mass density, μ and λ are the known Lamé parameters from classical elasticity, while J is the rotational inertial density, α , β , η and γ are extra material parameters from the micropolar model and representative of additional material points interactions see [19,43,44] for further discussion on the interpretation of these parameters.

Figure 15 presents the computed directionality curves for increasing porosity values, namely: 0.000, 0.196, 0.503 and 0.709. A porosity of 0.0 represents a homogeneous material, used as a reference in this case. As expected, the directionality of the material increases with porosity, and the higher values for the averaged group speed occur along the x and y axes where we have continuous paths for the wave to propagate [10]. Notice that the resulting curves are symmetric with respect to rotations of 90° . The same symmetry group can be seen in the unit cell.

For comparison, we present the isofrequency contours for the first three branches of the dispersion relations for this material in Figure 16 [19]. In this case we have different normalized frequency ranges — $\Omega \in [0, \Omega_{\max}]$ — when we change the porosity as the material becomes more dispersive when heterogeneity appears. Here, the normalized frequency is defined as

$$\Omega = \frac{2d\omega}{c_T},$$

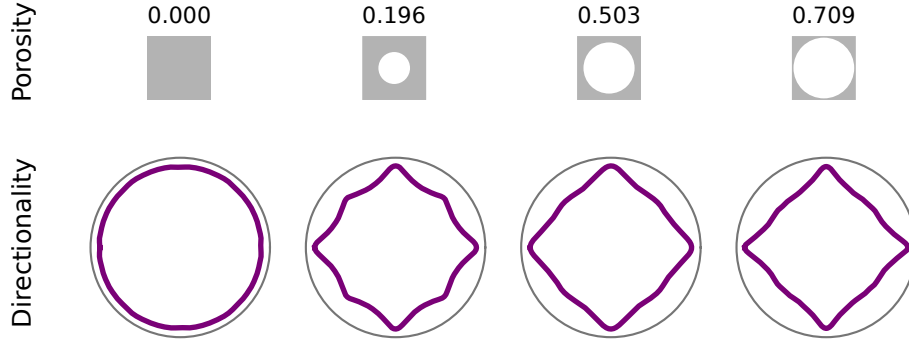


Figure 15. Directionality curves for a cellular material with increasing porosity.

where $c_T^2 = \mu/\rho$ is the phase speed of the transverse wave in the low frequency limit for the homogeneous case. The maximum normalized frequency (Ω_{\max}) in each case is 43.38, 46.92, 57.49, and 70.84.

6. Conclusions

We presented a method to visualize the directionality of waves in periodic materials modifying the work of Valencia et al. [10] and extending it to the three-dimensional case. This method takes as input dispersion (hyper-) surfaces obtained using a Bloch analysis and outputs a curve/surface with the bulk directionality encoded on it. As such, it can be used for dispersion curves obtained in different physical contexts such as elastodynamics or electrodynamics. The approach used in this work does not separate modes M_i and wave types; instead, it deals with several modes at once allowing to present the directionality for a broadband frequency range and not just the low-frequency limit, as is common. Our approach provides a qualitative tool that is useful to describe the global behavior of waves when propagating through the analyzed material; it is intended to be used as a complement to dispersion curves and surfaces.

References

- [1] Banerjee B. An Introduction to Metamaterials and Waves in Composites. 1st ed. Taylor & Francis; 2011.
- [2] Joannopoulos J, Johnson S, Winn J, et al. Photonic Crystals: Molding the Flow of Light. 2nd ed. Princeton University Press; 2008.
- [3] Deymier PA. Acoustic metamaterials and phononic crystals. Vol. 173. Springer Science & Business Media; 2013.
- [4] Norris AN, Haberman MR. Introduction to the special issue on acoustic metamaterials. The Journal of the Acoustical Society of America. 2012;132(4):2783–2783.
- [5] Hussein MI, Leamy MJ, Ruzzene M. Dynamics of phononic materials and structures: Historical origins, recent progress, and future outlook. Applied Mechanics Reviews. 2014; 66(4).
- [6] Goldsberry BM, Haberman MR. Negative stiffness honeycombs as tunable elastic metamaterials. Journal of Applied Physics. 2018;123(9):091711.

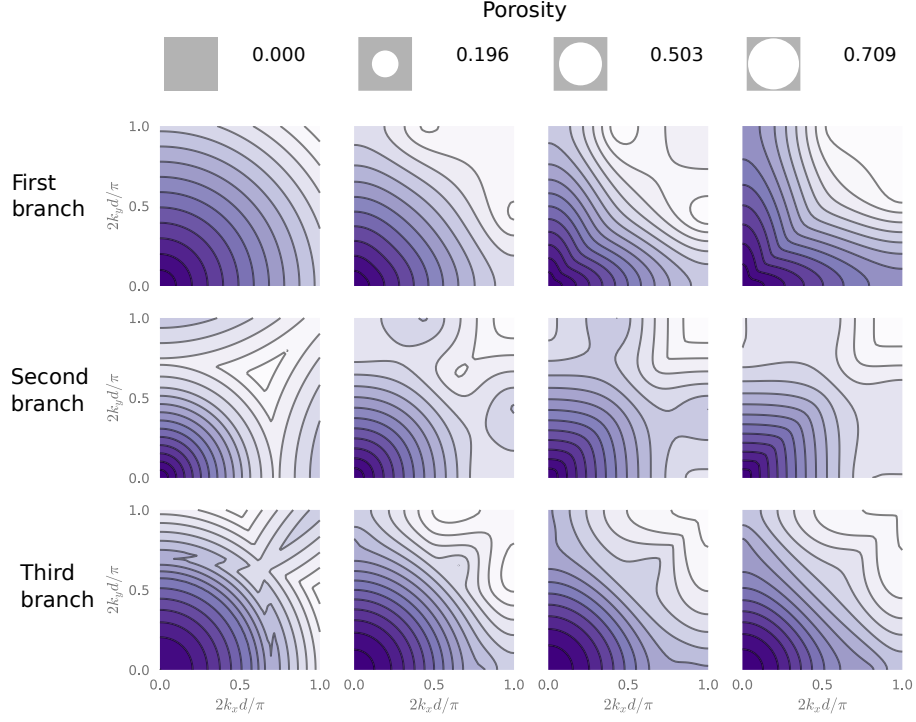


Figure 16. Curves of isofrequency for a cellular material with increasing porosity for the first three branches. These are the plots usually used to analyze directionality in periodic materials. The maximum normalized frequency in each case is 43.38, 46.92, 57.49, and 70.84

- [7] Milton GW, Cherkaev AV. Which elasticity tensors are realizable? Journal of Engineering Materials and Technology. 1995;.
- [8] Norris AN, Nagy AJ. Metal water: A metamaterial for acoustic cloaking. Proceedings of Phononics, Santa Fe, New Mexico, USA. 2011;:112–113.
- [9] Willis JR. Negative refraction in a laminate. Journal of the Mechanics and Physics of Solids. 2016;97:10–18.
- [10] Valencia C, Restrepo D, Mankame ND, et al. Computational characterization of the wave propagation behavior of multi-stable periodic cellular materials. Extreme Mechanics Letters. 2019;33:100565.
- [11] Guarín-Zapata N, Gómez J, Kisailus D, et al. Bandgap tuning in bioinspired helicoidal composites. Journal of the Mechanics and Physics of Solids. 2019 Oct;131:344–357. Available from: <https://linkinghub.elsevier.com/retrieve/pii/S0022509619302431>.
- [12] Sigalas MM, Garcia N. Theoretical study of three dimensional elastic band gaps with the finite-difference time-domain method. Journal of Applied Physics. 2000;87(6):3122–3125.
- [13] Pennec Y, Vasseur JO, Djafari-Rouhani B, et al. Two-dimensional phononic crystals: Examples and applications. Surface Science Reports. 2010;65(8):229–291.
- [14] Bloch F. Über die quantenmechanik der elektronen in kristallgittern. Zeitschrift für physik. 1929;52(7-8):555–600.
- [15] Brillouin L. Wave propagation in periodic structures: electric filters and crystal lattices. Courier Dover Publications; 2003.
- [16] Kittel C. Introduction to Solid State Physics. 7th ed. Wiley; 1996.
- [17] Zhang X, Liu Z. Negative refraction of acoustic waves in two-dimensional phononic crystals. Applied Physics Letters. 2004;85(2):341–343.
- [18] Valencia C, Gomez J, Guarín-Zapata N. A General-Purpose Element-Based Approach to Compute Dispersion Relations in Periodic Materials with Existing Finite Element Codes.

- Journal of Theoretical and Computational Acoustics. 2019 Jul;:1950005 Available from: <https://www.worldscientific.com/doi/abs/10.1142/S2591728519500051>.
- [19] Guarín-Zapata N, Gomez J, Valencia C, et al. Finite element modeling of micropolar-based phononic crystals. *Wave Motion*. 2020 Jan;92:102406. Available from: <https://linkinghub.elsevier.com/retrieve/pii/S0165212519300526>.
 - [20] Nye JF, et al. Physical properties of crystals: their representation by tensors and matrices. Oxford university press; 1985.
 - [21] Moakher M, Norris AN. The closest elastic tensor of arbitrary symmetry to an elasticity tensor of lower symmetry. *Journal of Elasticity*. 2006;85(3):215–263. Available from: <http://link.springer.com/article/10.1007/s10659-006-9082-0>.
 - [22] Maurin F, Claeys C, Deckers E, et al. Probability that a band-gap extremum is located on the irreducible Brillouin-zone contour for the 17 different plane crystallographic lattices. *International Journal of Solids and Structures*. 2018;135:26–36. Available from: <https://www.sciencedirect.com/science/article/pii/S0020768317305103>.
 - [23] Ruzzene M, Scarpa F, Soranna F. Wave beaming effects in two-dimensional cellular structures. *Smart materials and structures*. 2003;12(3):363.
 - [24] Ruzzene M, Scarpa F. Directional and band-gap behavior of periodic auxetic lattices. *physica status solidi (b)*. 2005;242(3):665–680.
 - [25] Zener C. Elasticity and anelasticity of metals. University of Chicago press; 1948.
 - [26] Kanit T, N’Guyen F, Forest S, et al. Apparent and effective physical properties of heterogeneous materials: Representativity of samples of two materials from food industry. *Computer Methods in Applied Mechanics and Engineering*. 2006;195(33):3960–3982.
 - [27] Ranganathan SI, Ostoja-Starzewski M. Universal elastic anisotropy index. *Physical Review Letters*. 2008;101(5):055504.
 - [28] Auld BA. Acoustic fields and waves in solids. Vol. 1. Wiley New York; 1973.
 - [29] Johnson SG. Notes on the algebraic structure of wave equations. Massachusetts Institute of Technology; 2010.
 - [30] Reddy J. Applied Functional Analysis and Variational Methods in Engineering. 1st ed. Krieger Publishing; 1991.
 - [31] Michel JC, Moulinec H, Suquet P. Effective properties of composite materials with periodic microstructure: a computational approach. *Computer methods in applied mechanics and engineering*. 1999;172(1-4):109–143.
 - [32] Sukumar N, Pask JE. Classical and enriched Finite element formulations for Bloch-periodic boundary conditions. *International Journal of Numerical Methods in Engineering*. 2009 2;77(8):1121–1138.
 - [33] Buchwald VT. Elastic waves in anisotropic media. *Proceedings of the Royal Society of London Series A Mathematical and Physical Sciences*. 1959;253(1275):563–580.
 - [34] Carcione JM. Wave fields in real media: Wave propagation in anisotropic, anelastic, porous and electromagnetic media. Elsevier; 2007.
 - [35] Thomsen L. Weak elastic anisotropy. *Geophysics*. 1986;51(10):1954–1966.
 - [36] Casadei F, Rimoli J. Anisotropy-induced broadband stress wave steering in periodic lattices. *International Journal of Solids and Structures*. 2013;50(9):1402–1414.
 - [37] Ledbetter H, Migliori A. A general elastic-anisotropy measure. *Journal of applied physics*. 2006;100(6):063516.
 - [38] Arfken GB, Weber HJ, Harris F. Mathematical Methods for Physicists. 6th ed. Academic Press; 2005.
 - [39] Schlömer N. meshzoo [<https://github.com/nschloe/meshzoo>]; 2020.
 - [40] Scopatz A, Huff KD. Effective computation in physics: Field guide to research with Python. O’Reilly Media, Inc.; 2015. Available from: <http://physics.codes/>.
 - [41] Virtanen P, Gommers R, Oliphant TE, et al. SciPy 1.0: fundamental algorithms for scientific computing in Python. *Nature methods*. 2020;17(3):261–272.
 - [42] Langlet P. Analyse de la propagation des ondes acoustiques dans les matériaux périodiques à l’aide de la méthode des éléments finis [dissertation]. Valenciennes; 1993.
 - [43] Lakes R. Experimental micro mechanics methods for conventional and negative Poisson’s

- ratio cellular solids as Cosserat continua. Journal of Engineering Materials and Technology. 1991;113(1):148–155.
- [44] Hassanpour S, Heppler GR. Micropolar elasticity theory: a survey of linear isotropic equations, representative notations, and experimental investigations. Mathematics and Mechanics of Solids. 2017;22(2):224–242.

Appendix A. Explicit form for the Christoffel equations

A.1. Three dimensions

For a triclinic material with a stiffness tensor given by

$$[C] = \begin{bmatrix} C_{11} & C_{12} & C_{13} & C_{14} & C_{15} & C_{16} \\ C_{12} & C_{22} & C_{23} & C_{24} & C_{25} & C_{26} \\ C_{13} & C_{23} & C_{33} & C_{34} & C_{35} & C_{36} \\ C_{14} & C_{24} & C_{34} & C_{44} & C_{45} & C_{46} \\ C_{15} & C_{25} & C_{35} & C_{45} & C_{55} & C_{56} \\ C_{16} & C_{26} & C_{36} & C_{46} & C_{56} & C_{66} \end{bmatrix},$$

in Voigt notation, a density ρ and a wavevector $\boldsymbol{\kappa}$, the equation that needs to be solved is [28]

$$\det \left(\|\boldsymbol{\kappa}\|^2 \begin{bmatrix} \alpha & \delta & \varepsilon \\ \delta & \beta & \xi \\ \varepsilon & \xi & \gamma \end{bmatrix} \begin{bmatrix} u_1 \\ u_2 \\ u_3 \end{bmatrix} - \rho\omega^2 \begin{bmatrix} 1 & 0 & 0 \\ 0 & 1 & 0 \\ 0 & 0 & 1 \end{bmatrix} \begin{bmatrix} u_1 \\ u_2 \\ u_3 \end{bmatrix} \right) = 0, \quad (\text{A1})$$

with

$$\begin{aligned} \alpha &= C_{11}n_1^2 + C_{66}n_2^2 + C_{55}n_3^2 + 2C_{56}n_1n_3 + 2C_{15}n_3n_1 + 2C_{16}n_1n_2, \\ \beta &= C_{66}n_1^2 + C_{22}n_2^2 + C_{44}n_3^2 + 2C_{24}n_2n_3 + 2C_{46}n_3n_1 + 2C_{26}n_1n_2, \\ \gamma &= C_{55}n_1^2 + C_{44}n_2^2 + C_{33}n_3^2 + 2C_{34}n_2n_3 + 2C_{35}n_3n_1 + 2C_{45}n_1n_2, \\ \delta &= C_{16}n_1^2 + C_{26}n_2^2 + C_{33}n_3^2 + (C_{46} + C_{25})n_2n_3 + (C_{14} + C_{56})n_3n_1 \\ &\quad + (C_{12} + C_{66})n_1n_2, \\ \varepsilon &= C_{15}n_1^2 + C_{46}n_2^2 + C_{35}n_3^2 + (C_{45} + C_{36})n_2n_3 + (C_{13} + C_{55})n_2n_1 \\ &\quad + (C_{14} + C_{56})n_1n_2, \\ \xi &= C_{56}n_1^2 + C_{24}n_2^2 + C_{34}n_3^2 + (C_{44} + C_{23})n_2n_3 + (C_{36} + C_{45})n_3n_1 \\ &\quad + (C_{25} + C_{46})n_1n_2, \end{aligned}$$

where $\hat{\mathbf{n}} = (n_1, n_2, n_3) = \frac{\boldsymbol{\kappa}}{\|\boldsymbol{\kappa}\|}$.

In the case of orthotropic materials aligned with the coordinate system these ex-

pressions can be simplified to

$$\begin{aligned}
\alpha &= C_{11}n_1^2 + C_{66}n_2^2 + C_{55}n_3^2, \\
\beta &= C_{66}n_1^2 + C_{22}n_2^2 + C_{44}n_3^2, \\
\gamma &= C_{55}n_1^2 + C_{44}n_2^2 + C_{33}n_3^2, \\
\delta &= (C_{12} + C_{66})n_1n_2, \\
\varepsilon &= (C_{13} + C_{55})n_3n_1, \\
\xi &= (C_{44} + C_{23})n_2n_3,
\end{aligned}$$

this can be further simplified for cubic materials.

$$\begin{aligned}
\alpha &= C_{11}n_1^2 + C_{44}(1 - n_1^2), \\
\beta &= C_{11}n_2^2 + C_{44}(1 - n_2^2), \\
\gamma &= C_{11}n_3^2 + C_{44}(1 - n_3^2), \\
\delta &= (C_{12} + C_{44})n_1n_2, \\
\varepsilon &= (C_{12} + C_{44})n_3n_1, \\
\xi &= (C_{12} + C_{44})n_2n_3.
\end{aligned}$$

For materials with transversely isotropic symmetry the equations can be solved analytically [34]. For a wave propagating in the plane 1-3, and taking $n_2 = 0$, we have

$$\begin{aligned}
\omega_{\text{qP}}^2 &= \frac{\|\boldsymbol{\kappa}\|^2(C_{11}n_1^2 + C_{33}n_3^2 + C_{55} + \sqrt{M})}{2\rho}, \\
\omega_{\text{qS}}^2 &= \frac{\|\boldsymbol{\kappa}\|^2(C_{11}n_1^2 + C_{33}n_3^2 + C_{55} - \sqrt{M})}{2\rho}, \\
\omega_{\text{S}}^2 &= \frac{\|\boldsymbol{\kappa}\|^2(C_{66}n_1^2 + C_{55}n_3^2)}{\rho}, \\
M &= [(C_{11} - C_{55})n_1^2 + (C_{55} - C_{33})n_3^2]^2 + 4[(C_{13} + C_{55})^2n_1n_3]^2.
\end{aligned}$$

A.2. Two dimensions

In the case of a monoclinic material, we could align the symmetry plane to obtain the following two-dimensional problem

$$\det \left(\|\boldsymbol{\kappa}\|^2 \begin{bmatrix} \alpha & \delta \\ \delta & \beta \end{bmatrix} - \rho\omega^2 \begin{bmatrix} 1 & 0 \\ 0 & 1 \end{bmatrix} \right) = 0,$$

that can be solved analytically as

$$\omega^2 = \frac{\|\boldsymbol{\kappa}\|^2}{2\rho} [\alpha + \beta \pm \sqrt{(\alpha - \beta)^2 + 4\delta^2}]$$

with

$$\begin{aligned}\alpha &= C_{11}n_1^2 + C_{66}n_2^2 + 2C_{16}n_1n_2, \\ \beta &= C_{66}n_1^2 + C_{22}n_2^2 + 2C_{26}n_1n_2, \\ \delta &= C_{16}n_1^2 + C_{26}n_2^2 + (C_{12} + C_{66})n_1n_2,\end{aligned}$$

that reduces to

$$\begin{aligned}\alpha &= C_{11}n_1^2 + C_{66}n_2^2, \\ \beta &= C_{66}n_1^2 + C_{22}n_2^2, \\ \delta &= (C_{12} + C_{66})n_1n_2,\end{aligned}$$

for orthotropic materials and

$$\begin{aligned}\alpha &= C_{11}n_1^2 + C_{66}n_2^2, \\ \beta &= C_{66}n_1^2 + C_{11}n_2^2, \\ \delta &= (C_{12} + C_{66})n_1n_2,\end{aligned}$$

for cubic materials.

Appendix B. Material properties

In the following, we present the properties used in the paper.

B.1. Two dimensions

- Aluminum:

$$[C] = \begin{bmatrix} 112.35 & 60.49 & 0 \\ 60.49 & 112.35 & 0 \\ 0 & 0 & 25.9 \end{bmatrix} \text{ GPa}, \quad \rho = 2700 \text{ kg/m}^3.$$

- GaAs:

$$[C] = \begin{bmatrix} 118.8 & 59.4 & 0 \\ 59.4 & 118.8 & 0 \\ 0 & 0 & 53.7 \end{bmatrix} \text{ GPa}, \quad \rho = 5320 \text{ kg/m}^3.$$

- Graphite:

$$[C] = \begin{bmatrix} 235 & 3.69 & 0 \\ 3.69 & 26 & 0 \\ 0 & 0 & 28.2 \end{bmatrix} \text{ GPa}, \quad \rho = 1790 \text{ kg/m}^3.$$

B.2. Three dimensions

- Aluminum:

$$[C] = \begin{bmatrix} 112.35 & 60.49 & 60.49 & 0 & 0 & 0 \\ 60.49 & 112.35 & 60.49 & 0 & 0 & 0 \\ 60.49 & 60.49 & 112.35 & 0 & 0 & 0 \\ 0 & 0 & 0 & 25.9 & 0 & 0 \\ 0 & 0 & 0 & 0 & 25.9 & 0 \\ 0 & 0 & 0 & 0 & 0 & 25.9 \end{bmatrix} \text{ GPa}, \quad \rho = 2700 \text{ kg/m}^3.$$

- β -brass:

$$[C] = \begin{bmatrix} 52 & 27.5 & 27.5 & 0 & 0 & 0 \\ 27.5 & 52 & 27.5 & 0 & 0 & 0 \\ 27.5 & 27.5 & 52 & 0 & 0 & 0 \\ 0 & 0 & 0 & 173 & 0 & 0 \\ 0 & 0 & 0 & 0 & 173 & 0 \\ 0 & 0 & 0 & 0 & 0 & 173 \end{bmatrix} \text{ GPa}, \quad \rho = 7600 \text{ kg/m}^3.$$

- Cadmium:

$$[C] = \begin{bmatrix} 115.9 & 41.05 & 41 & 0 & 0 & 0 \\ 41.05 & 115.9 & 41 & 0 & 0 & 0 \\ 41 & 41 & 51.2 & 0 & 0 & 0 \\ 0 & 0 & 0 & 19.95 & 0 & 0 \\ 0 & 0 & 0 & 0 & 19.95 & 0 \\ 0 & 0 & 0 & 0 & 0 & 37.43 \end{bmatrix} \text{ GPa}, \quad \rho = 8650 \text{ kg/m}^3.$$

- Carbon-Epoxy:

$$[C] = \begin{bmatrix} 12.37 & 6.15 & 6.19 & 0 & 0 & 0 \\ 6.15 & 21.37 & 6.19 & 0 & 0 & 0 \\ 6.19 & 6.19 & 146.30 & 0 & 0 & 0 \\ 0 & 0 & 0 & 4.80 & 0 & 0 \\ 0 & 0 & 0 & 0 & 4.80 & 0 \\ 0 & 0 & 0 & 0 & 0 & 3.11 \end{bmatrix} \text{ GPa}, \quad \rho = 1900 \text{ kg/m}^3.$$